Unique properties of the 11-*cis* and 11,11′-di-*cis* isomers of β-carotene as revealed by electronic absorption, resonance Raman and ^{1}H and ^{13}C NMR spectroscopy and by HPLC analysis of their thermal isomerization

Ying Hu,[a] Hideki Hashimoto,[b] Gérard Moine,[c] Urs Hengartner[c] and Yasushi Koyama*,[a]

[a] *Faculty of Science, Kwansei Gakuin University, Uegahara, Nishinomiya 662, Japan*
[b] *Department of Materials Science and Chemical Engineering, Faculty of Engineering, Shizuoka University, 5-1, Johoku 3-Chome, Hamamatsu 432, Japan*
[c] *Vitamins and Fine Chemicals Division, F. Hoffmann-La Roche Ltd, CH-4070 Basel, Switzerland*

In comparison with the all-*trans* and other *cis* isomers of β-carotene, the 11-*cis* and 11,11′-di-*cis* isomers exhibited the following unique properties. (1) The wavelengths of the $B_u^+ \leftarrow A_g^-$ (0–0) absorption of these two isomers are similar to that of the all-*trans* isomer, and do not follow the general rule of its blue shift found in other mono-*cis* and di-*cis* isomers. Their extinction coefficients are significantly lower than those of other isomers. (2) The frequencies of the C=C stretching Raman lines of these isomers are the same as that of the all-*trans* isomer, and do not follow the general trend of high-frequency shifts found in other mono-*cis* and di-*cis* isomers. The Raman lines due to the out-of-plane C–H wagging and methyl rocking modes appear in the 11,11′-di-*cis* isomer. (3) The ^{1}H chemical shifts of these isomers indicate severe steric interaction between the methyl and the olefinic ^{1}H atoms in the concave side of the 11-*cis* bend, whereas their ^{13}C chemical shifts suggest twisting and polarization of the *cis* C11=C12 bond. (4) The rates of thermal isomerization of these isomers are much higher than that of the 15-*cis* isomer, *i.e.* the least stable isomer previously known.

The results lead us to the conclusion that the 11-*cis* configuration has inherent twisting around the double and single bonds in the *cis* bend due to the severe steric interaction between the 13-methyl and the 10-olefinic hydrogens, and that it is unstable enough to disappear thermally at room temperature.

Introduction

15-*cis*-Carotenoids are bound to the reaction centres (RCs) of purple photosynthetic bacteria and spinach, and are suspected of playing an important role in the photoprotective function:[1–3] For example, the 15-*cis* isomers of spheroidene, neurosporene and spirilloxanthin are bound to the RCs of *Rhodobacter sphaeroides* 2.4.1, *Rhb. sphaeroides* G1C and *Rhodospirillum rubrum* S1, respectively (for a review, see ref. 1), whereas 15-*cis*-β-carotene (see Fig. 1 for the configurations of isomeric β-carotenes) is bound to the RCs of spinach photosystem II[4] and photosystem I.[5] A unique property of 15-*cis*-β-carotene is the extremely efficient, one-way isomerization into all-*trans*-β-carotene *via* the T_1 state (see ref. 2), and this property has been related to the photo-protective function of the carotenoids.[2,3] On the other hand, 11-*cis* retinal is bound to rhodopsin as the protonated Schiff base, and the 11-*cis* to all-*trans* isomerization *via* the S_1 state triggers the primary process of vision.[6,7] The reason for the selection of the particular *cis* isomers is, most probably, the efficient isomerization toward the all-*trans* isomer *via* the excited states.

It is intriguing to address the question, from this viewpoint, as to why no 11-*cis* configuration has been found in the natural carotenoids, and the 15-*cis* configuration, instead, is used for the physiological function. Zechmeister ascribed the absence of the 11-*cis* configuration to the apparent instability of the unmethylated-*cis* configurations (7-*cis* and 11-*cis*) due to the severe steric hindrance in the concave side of the *cis* bend.[8] However, this reasoning is not complete in the sense that it does not explain why the 7-*cis*[9] and 11-*cis*[10] isomers of retinal can be produced photolytically in polar solvents from the all-*trans* isomer. It does not explain, even in the case of carotenoids, why the 7-*cis* isomer can be produced thermally in β-carotene[11] and photolytically in β-apo-8′-carotenal.[12]

Since an obvious difference between the carotenoids and the retinoids lies in the length of the conjugated chain, we have been identifying a set of *cis* isomers which can be produced from the all-*trans* isomer in a series of aldehydes having similar chemical structures but different lengths of the conjugated chain. The 11-*cis* isomer was found in retinal (C_{20} aldehyde), 2,7-dimethyl-9-(2,6,6-trimethylcyclohex-1-enyl)nona-2,4,6,8-tetraenal ($C_{20'}$ aldehyde),[13] and retinylideneacetaldehyde (C_{22} aldehyde);[14] however, it was not found in β-apo-12′-carotenal (C_{25} aldehyde),[15] 3,7,11-trimethyl-13-(2,6,6-trimethylcyclohex-1-enyl)trideca-2,4,6,8,10,12-hexenal ($C_{25'}$ aldehyde),[13] and β-apo-8′-carotenal (C_{30} aldehyde).[12] Since the 11-*cis* isomer has been found not in aldehydes having seven or more conjugated C=C bonds (in addition to the terminal C=O bond) but in aldehydes having six or less conjugated C=C bonds, the key factor determining the presence or absence of the 11-*cis* isomer must be the length of the conjugated chain which affects the electronic and molecular structure.

Another approach to determining the reason why the 11-*cis*-configuration has not been found in the carotenoids having a longer conjugated chain is to examine and characterize an 11-*cis* carotenoid, if it is stable enough to be isolated. From this viewpoint, we have attempted to synthesize the 11-*cis* and 11,11′-di-*cis* isomers of β-carotene, to identify their unique properties in comparison with those of the rest of the *cis*–*trans* isomers, and to determine the reason why these isomers have not been found in nature. We have applied electronic-absorption, resonance-Raman and ^{1}H and ^{13}C

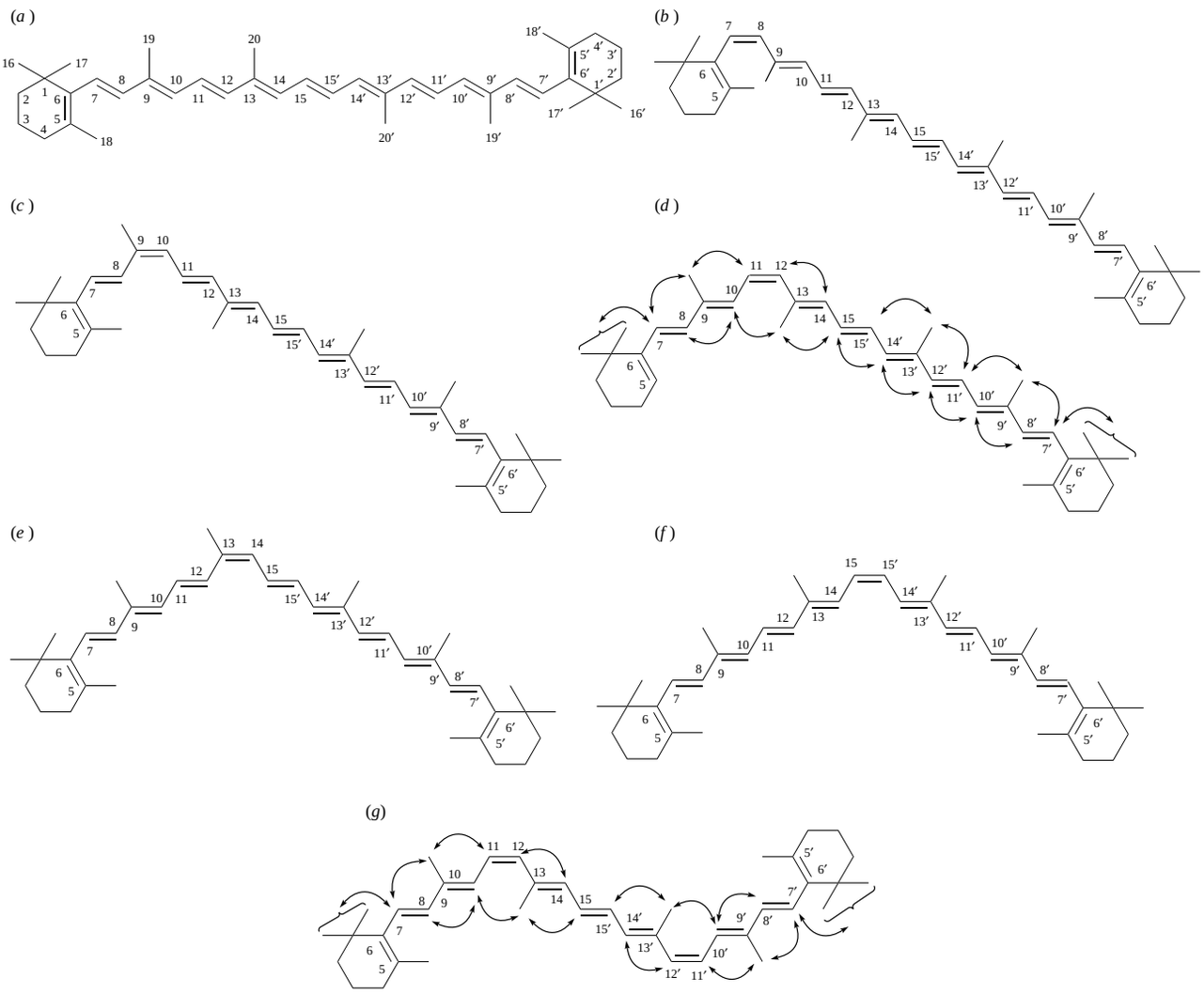

Fig. 1 Configurations of isomeric β-carotenes (schematic presentation) and numbering of carbon atoms; the (*a*) all-*trans*, (*b*) 7-*cis*, (*c*) 9-*cis*, (*d*) 11-*cis*, (*e*) 13-*cis*, (*f*) 15-*cis* and (*g*) 11,11′-di-*cis* isomers. Observed NOE correlations are shown for the 11-*cis* and 11,11′-di-*cis* isomers. Each methyl group will be referred to, in the text, by the numbering of the carbon atom to which it is attached.

NMR spectroscopy to these isomers, and traced their thermal isomerization by HPLC.

Concerning the other *cis–trans* isomers of β-carotene, the results of electronic-absorption,[16,17] resonance-Raman[17,18] and ^{1}H NMR spectroscopy[19] as well as that of thermal isomerization[20] have been published. A comparative study on the ground-state energies of the all-*trans* and all the mono-*cis* isomers and on thermal isomerization of the all-*trans*, 13-*cis* and 15-*cis* isomers has been published recently.[21]

Results and discussion

HPLC elution profiles and structural identification of the 11-*cis* and 11,11′-di-*cis* isomers

Fig. 2 compares the HPLC elution profiles of purified (*a*) 11-*cis* and (*b*) 11,11′-di-*cis*-β-carotenes with (*c*) those of isomeric mixtures of β-carotene which were obtained by thermal isomerization, *i.e.* heating *in vacuo* the all-*trans* crystals to the melting point, 183 °C, and (*d*) by I_2-sensitized photo-isomerization of the all-*trans* isomer in *n*-hexane. Assignment of each peak in the elution profiles (*c*) and (*d*) is based on structural determination by ^{1}H NMR spectroscopy[16,19,22] and also on the results of thermal- and photo-isomerization.[20] I_2-sensitized photo-isomerization produces only the methylated-*cis* (9-*cis* and 13-*cis*) configurations, and thermal isomerization produces additionally a pair of unmethylated-*cis* (7-*cis* and 15-*cis*) configurations.

Comparison of the elution profiles leads us to two important conclusions. (1) The 11-*cis* and 11,11′-di-*cis* isomers can be purified practically up to 100% (at least when detected at the 450 nm main absorption). (2) It is highly unlikely that the 11-*cis* or the 11,11′-di-*cis* isomer can be produced either thermally or photolytically starting from the all-*trans* isomer. The possibility that a weak peak of the 11-*cis* isomer is hidden in the skirt of the 9,15-*cis* isomer cannot be excluded completely, but it will be shown to be unlikely after examination of thermal isomerization starting from the 11-*cis* isomer (*vide infra*).

The structures of the 11-*cis* and 11,11′-di-*cis* isomers [Fig. 1(*d*) and (*g*)] were confirmed by ^{1}H NMR spectroscopy using (1) the 'isomerization shifts', which are defined as changes in the chemical shifts on going from the all-*trans* isomer to a particular *cis* isomer, and (2) the nuclear Overhauser effect (NOE) correlations: Table 1 lists the chemical shifts of ^{1}H (hereafter, abbreviated as H) for the all-*trans*, 11-*cis*, 11,11′-di-*cis* and 15-*cis* isomers; the 'isomerization shifts' are shown in parentheses. When a *cis* bend is introduced, high-field-shifts (hereafter abbreviated as hfs) take place on the convex side, whereas low-field-shifts (lfs) take place on the concave side due to changes in the steric interaction among Hs. On this basis, a set of observations, *i.e.* the hfs of 11H and 12H, the lfs of 13Me and 10H, and the rest of the signals remain almost unchanged (except for the lfs of 14H), identify one single 11-*cis* configuration in the 11-*cis* isomer. The number of observed H signals which is reduced to one half in the 11,11′-di-*cis* isomer indicates that each pair of Hs on both sides of the conjugated skeleton is located in a similar environment. The hfs of 11H (11′H) and

Table 1 The H chemical shifts (isomerization shifts) of the all-*trans*-, 11-*cis*-, 11,11′-di-*cis*- and 15-*cis*-β-carotenes in [$^2H_6$]benzene (ppm)

Proton	all-*trans*	11-*cis*	11,11′-di-*cis*	15-*cis*	Proton	all-*trans*	11-*cis*	11,11′-di-*cis*	15-*cis*
1Me 1′Me	1.17	1.13 (−0.04) 1.16 (−0.01)	1.13 (−0.04)	1.15 (−0.02)	7H 7′H	6.34	6.34	6.33 (−0.01)	6.33 (−0.01)
5Me 5′Me	1.84	1.77 (−0.07) 1.83 (−0.01)	1.76 (−0.08)	1.81 (−0.03)	8H 8′H	6.43	6.41 (−0.02)	6.40 (−0.03)	6.40 (−0.03)
9Me 9′Me	1.94	1.90 (−0.04) 1.93 (−0.01)	1.90 (−0.04)	1.93 (−0.01)	10H 10′H	6.37	7.00 (+0.63) 6.36 (−0.01)	6.98 (+0.61)	6.37
13Me 13′Me	1.87	2.03 (+0.16) 1.82 (−0.05)	1.97 (+0.10)	1.87	11H 11′H	6.81	6.47 (−0.34) 6.79 (−0.02)	6.46 (−0.35)	6.82 (+0.01)
2H 2′H	1.50	1.49 (−0.01) 1.50	1.48 (−0.02)	1.50	12H 12′H	6.50	6.13 (−0.37) 6.49 (−0.01)	6.12 (−0.38)	6.50
3H 3′H	1.61	1.60 (−0.01) 1.61	1.59 (−0.02)	1.60 (−0.01)	14H 14′H	6.33	6.46 (+0.13) 6.28 (−0.05)	6.41 (+0.08)	6.88 (+0.55)
4H 4′H	1.99	1.97 (−0.02) 1.98 (−0.01)	1.95 (−0.04)	1.98 (−0.01)	15H 15′H	6.70	6.64 (−0.06)	6.58 (−0.12)	6.47 (−0.23)

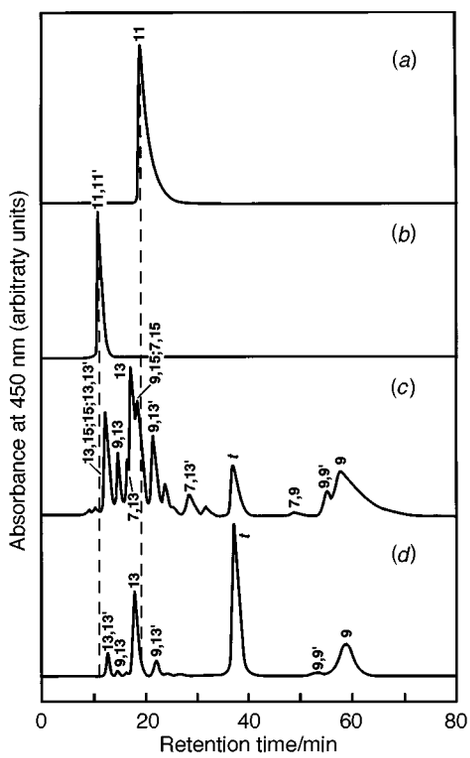

Fig. 2 HPLC elution profiles of the (*a*) 11-*cis* and (*b*) 11,11′-di-*cis* isomers and those of isomeric mixtures obtained (*c*) by thermal isomerization and (*d*) by I_2-sensitized photo-isomerization starting from the all-*trans* isomer

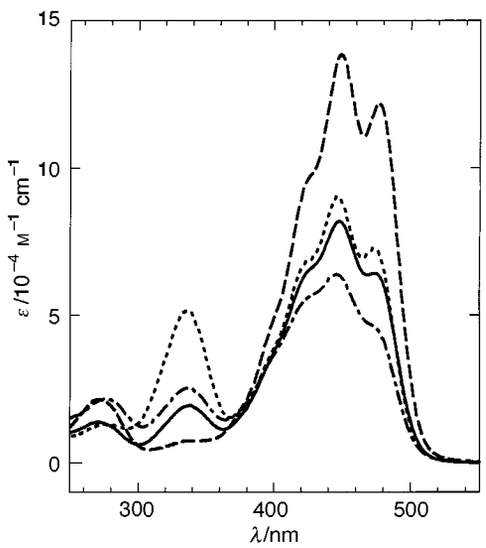

Fig. 3 Electronic absorption spectra of the all-*trans* (---), 15-*cis* (···), 11-*cis* (——) and 11,11′-di-*cis* (–·–·) isomers; in *n*-hexane, at room temperature

12H (12′H) as well as the lfs of 13Me and 10H (13′Me and 10′H) indicate the presence of a pair of 11-*cis* configurations. The rest of the chemical shifts of this isomer are similar to that of the all-*trans* isomer, indicating the presence of three all-*trans* fragments in this di-*cis* isomer. The ^1H NMR spectra of the all-*trans*, 7-*cis*, 9-*cis*, 13-*cis* and 15-*cis* isomers for comparison were reported previously.[19]

Fig. 1(*d*) and (*g*) show the NOE correlations observed for the above set of *cis* isomers. The correlation between 10H and 13Me in the 11-*cis* isomer (the correlations between 10H and 13Me as well as between 10′H and 13′Me in the 11,11′-di-*cis* isomer) confirms the presence of the 11-*cis* configuration(s). The NOE correlations between 1Me and 7H (as well as between 1′Me and 7′H) guarantee the s-*cis* configuration around the 6C–7C (and 6′C–7′C) axis for the 11-*cis* (11,11′di-*cis*) isomer. The rest of the NOE correlations identify the all-*trans* fragments in these isomers.

Unique electronic absorption spectra of the 11-*cis* and 11,11′-di-*cis* isomers

Fig. 3 compares the electronic absorption spectra of the 11-*cis* (solid line) and 11,11′-di-*cis* (dotted-broken line) isomers with those of the all-*trans* (broken line) and the 15-*cis* (dotted line) isomers. The electronic absorption spectrum of the 11-*cis* isomer exhibits the wavelength of the main $B_u^+ \leftarrow A_g^-$ absorption similar to those of the all-*trans* and the 15-*cis* isomers, but it shows a lower molar extinction coefficient of the particular absorption. On the other hand, the spectrum of the 11,11′-di-*cis* isomer exhibits a similar wavelength of the $B_u^+ \leftarrow A_g^-$ absorption and a considerably lower molar extinction coefficient. (The symmetry notation, *i.e.* A_g^-, A_g^+ and B_u^+, can be used in a strict sense for isomers with C_{2h} symmetry such as planar all-*trans*- and 11,11′-di-*cis*-β-carotenes. However, we will use this notation for other isomers for convenience in correlating singlet states.) Table 2 compares (1) the wavelengths of the $A_g^+ \leftarrow A_g^-$ absorption (called '*cis*-peak') and the $B_u^+ \leftarrow A_g^-$ absorption ('main peak'), (2) the molar extinction coefficients at the maximum of the $B_u^+ \leftarrow A_g^-$ absorption (defined as ε), and (3) the relative intensities of the $A_g^+ \leftarrow Ag^-$ *vs.* $B_u^+ \leftarrow A_g^-$ absorption for all the *cis–trans* isomers whose structures have been determined. It is known that the $B_u^+ \leftarrow A_g^-$ (0–0) absorption exhibits a general rule of blue shift in the order: all-*trans*, peripheral mono-*cis* (7-*cis* and 9-*cis*), central mono-*cis* (13-*cis*) and then di-*cis* (9,13-, 9,13′-, 9,15- and 13,15-di-*cis*).[17] This general trend was explained in terms of reduced conjugation when the *cis* configuration is introduced into the conjugated chain (one *cis* configuration from the periphery to the centre in the mono-*cis* isomers, and then, two of them in the di-*cis* isomers). The 15-*cis* isomer does not follow this rule; this observation may be ascribed to the C_{2v}

Table 2 The wavelengths of electronic absorptions, the molar extinction coefficient of the $B_u^+ \leftarrow A_g^-$ transition (ε), the relative intensity of the $A_g^+ \leftarrow A_g^-$ *vs.* $B_u^+ \leftarrow A_g^-$ absorption and the frequency of the 'C=C stretching' vibration for each isomeric β-carotene

	Electronic absorption/nm			$\varepsilon/10^{-5}$ dm^3 mol^{-1} cm^{-1}		Relative intensity $A_g^+ \leftarrow A_g^-$	
		$B_u^+ \leftarrow A_g^-$					'C=C stretching'
Isomer	$A_g^+ \leftarrow A_g^-$	(1–0)	(0–0)	Tsukida[a]	Present work	$B_u^+ \leftarrow A_g^-$	frequency/cm^{-1}
all-*trans*[a]	337[a]	450[a]	478[c]	1.390	1.33	0.06[c]	1529[c]
7-*cis*[a]	337[a]	446[a]	474[c]	1.387		0.06[c]	1530[c]
9-*cis*[a]	338[a]	445[a]	473[c]	1.297		0.09[c]	1534[c]
11-*cis*	338	448	475		0.818	0.25	1529
13-*cis*[a]	336[a]	442[a]	467[c]	1.073		0.36[c]	1542[c]
15-*cis*[a]	335[a]	448[a]	475[c]	1.032	0.903	0.52[c]	1539[c]
7,13′-di-*cis*[a]	334[a]	448[a]	—	1.117		0.25[c]	—
9,13′-di-*cis*[a,b]	335[a]	439[a]	465[c]	1.198		0.17[c]	1543[c]
9,15-di-*cis*[a]	334[a]	441[a]	468[c]	1.095		0.20[c]	1543[c]
11,11′-di-*cis*	337	446	475		0.639	0.40	1529
13,15-di-*cis*[a]	339[a]	436[a]	463[c]	1.043		0.14[c]	1548[c]

[a] Ref. 16. [b] Ref. 22. [c] Ref. 17.

(C_2) symmetry of this particular isomer, which can cause electronic coupling between the identical structures on both sides of the central *cis* bend. The above reasoning does not explain the wavelengths of the $B_u^+ \leftarrow A_g^-$ absorption of the present 11-*cis* and 11,11′-di-*cis* isomers, which are similar to that of the all-*trans* (15-*cis*) isomer.

It is also known that the molar extinction coefficient of the $B_u^+ \leftarrow A_g^-$ absorption (ε) decreases in the order: all-*trans* > 7-*cis* > 9-*cis* > 13-*cis* and then 15-*cis*, and the relative intensity of the $A_g^+ \leftarrow A_g^-$ *vs.* $B_u^+ \leftarrow A_g^-$ absorption increases in the same order.[16,17] These trends are naturally expected when one considers that the $B_u^+ \leftarrow A_g^-$ ($A_g^+ \leftarrow A_g^-$) transition moment is parallel (perpendicular) to the long-axis of each isomer. In comparison with the above trend of mono-*cis* isomers, the ε value of the 11-*cis* isomer is low and the $A_g^+ \leftarrow A_g^-$ *vs.* $B_u^+ \leftarrow A_g^-$ relative intensity is slightly higher than expected for this configuration. On the other hand, the 11,11′-di-*cis* isomer exhibits very weak $B_u^+ \leftarrow A_g^-$ absorption and very strong $A_g^+ \leftarrow A_g^-$ absorption for a di-*cis* isomer. As a result, the relative intensity ($A_g^+ \leftarrow A_g^-$ *vs.* $B_u^+ \leftarrow A_g^-$) becomes extremely high in comparison with other di-*cis* isomers.

Thus, the unique electronic absorption properties of the 11-*cis* isomer can be summarized as the comparatively long wavelength as well as the low oscillator strength of the $B_u^+ \leftarrow A_g^-$ transition for a mono-*cis* isomer. The properties of the 11,11′-di-*cis* isomer can be summarized as the extremely long wavelength and low oscillator strength of the $B_u^+ \leftarrow A_g^-$ transition and the high oscillator strength of the $A_g^+ \leftarrow A_g^-$ transition for a di-*cis* isomer. These results strongly suggest an anomaly, in the electronic and molecular structure(s) of the isomer(s), which cannot be explained in terms of planar *cis* configuration(s).

PPP-CI calculations on a model polyene, octadecanonaene ($C_{18}H_{20}$), showed that the main $B_u^+ \leftarrow A_g^-$ absorption shifts to the longer wavelength and its oscillator strength decreases when a (central) double bond is twisted (irrespective of *cis* or *trans* configuration). On the other hand, the particular absorption shifts to the shorter wavelength and its oscillator strength decreases when a (central) single bond is twisted. The results indicate that the wavelengths of the $B_u^+ \leftarrow A_g^-$ absorption of the 11-*cis* and 11,11′-di-*cis* isomers which are similar to that of the all-*trans* isomer as well as their oscillator strengths which are much lower than those of the other isomers can generally be attributed to the twisting of the conjugated backbone around both the double and the single bonds.

The PPP-CI calculation on the 5,13-di-*cis* isomer of the above model polyene with a twisted conformation around the 5-*cis* and 13-*cis* bonds (this corresponds to twisting around the 11-*cis* and 11′-*cis* double bonds in the 11,11′-di-*cis* isomer of β-carotene) showed that this isomer gives rise to the $A_g^+ \leftarrow A_g^-$ absorption for a molecular conformation, not with C_{2h} or C_i symmetry, but with C_2 symmetry (this result was anticipated by symmetry considerations). Further, twisting around the 6s and 12s bonds (this corresponds to twisting around the C12–C13 and C12′–C13′ bonds in 11,11′-di-*cis*-β-carotene) caused a large enhancement of the $A_g^+ \leftarrow A_g^-$ absorption. Therefore, our observation of the strong $A_g^+ \leftarrow A_g^-$ absorption in the 11,11′-di-*cis* isomer can be regarded as strong evidence for the C_2 symmetry of this isomer and for the twisting around both the C11=C12 (C11′=C12′) and the C12–C13 (C12′–C13′) bonds. However, an attempt to detect the optical activity of this isomer by measuring its circular dichroism was unsuccessful, suggesting the presence of equivalent amounts of antipodes in the solution.

Furthermore, the PPP-CI calculation on the 5,13-di-*cis* isomer of the model polyene in C_2 symmetry with twisting around both the double and the single bonds (for both the same and opposite directions) suggests the following characteristics of the electronic absorption spectrum of the 11,11′-di-*cis* isomer: (1) the wavelength of the $B_u^+ \leftarrow A_g^-$ absorption being similar to that of the all-*trans* isomer; (2) the extremely low oscillator strength of the $B_u^+ \leftarrow A_g^-$ absorption in comparison to all the other *cis–trans* isomers; and (3) the very high oscillator strength of the $A_g^+ \leftarrow A_g^-$ absorption when compared to other di-*cis* isomers.

Thus, the above PPP-CI calculations have qualitatively explained the electronic-absorption characteristics of the 11-*cis* and the 11,11′-di-*cis* isomers. However, more sophisticated calculations taking the σ-electrons into account are necessary for quantitative discussion.

Unique resonance Raman spectra of the 11-*cis* and 11,11′-di-*cis* isomers

Fig. 4 shows the Raman spectra of the (*a*) all-*trans*, (*b*) 11-*cis* and (*c*) 11,11′-di-*cis* isomers; the Raman spectra were recorded under pre-resonance conditions (see Experimental). Table 3 lists the assignments of the Raman lines based on the normal-coordinate calculations using a set of force constants which were determined by Saito and Tasumi;[23] reference was also made to the results of the normal-coordinate analysis of the Raman and infrared spectra of the all-*trans*, 7-*cis*, 9-*cis*, 13-*cis* and 15-*cis* isomers of β-carotene.[18]

The Raman lines characteristic of the 11-*cis* configuration can be more clearly seen in the 11,11′-di-*cis* isomer having C_2 symmetry, because Raman-active A-type vibrations can be generated as a linear combination of a pair of vibrations which are taking place on both sides of the conjugated chain. The Raman lines due to the in-plane vibrations of this di-*cis* isomer can be assigned as follows based on preliminary results of a normal-coordinate calculation: (1) The calculation showed that both

Table 3 Assignment of the Raman lines of all-*trans*-, 11-*cis*- and 11,11′-di-*cis*-β-carotenes

all-*trans*[a]		11-*cis*		11,11′-di-*cis*[a]	
				1577 (w)	
1529 (s)[b]	'C=C str'[c]	1529 (s)	'C=C str'	1529 (s)	'C=C str'
1447 (w)	Me asym def	1447 (w)	Me asym def	1447 (w)	Me asym def
1392 (vw)	Me sym def	1395 (w)	Me sym def	1395 (w)	Me sym def
1274 (w)	UT mode				
		1268 (w)	UC mode	1268 (m)	UC mode
1217 (w)	MT mode				
		1205 (m)	C12′–C13′ str	1197 (s)	C12–C13 str
1192 (m)	C8–C9 str	1192 (m)	C8′–C9′ str		
		1177 (m)	C14–C15 and		
1160 (s)	C14–C15 str	1158 (s)	C14′–C15′ str	1155 (m)	C14–C15 and C10–C11 str
				1085 (w)	13Me op rock
1025 (w)	9Me ip rock	1020 (w)	9Me ip rock	1018 (w)	9Me ip rock
1007 (s)	13Me ip rock	1007 (m)	13′Me ip rock		
		990 (w)	13Me ip rock	998 (m)	13Me ip rock
966 (w)	14H, 15H op wag	966 (w)	14H, 15H op wag	966 (w)	15H, 11H and 12H op wag
				822 (w)	11H, 12H op wag

[a] Vibrations taking place on one side of the conjugated chain, *i.e.* C8–C9, C10–C11, C12–C13, C14–C15, 9Me, 13Me, 11H, 12H, 14H and 15H, alone are shown; they include those on the other side, *i.e.* C8′–C9′, C10′–C11′, C12′–C13′, C14′–C15′, 9′Me, 13′Me, 11′H, 12′H, 14′H and 15′H. [b] s, m, w and vw stand for strong, medium, weak and very weak Raman lines. [c] The normal modes are abbreviated as str, stretching(s); def, deformation(s); rock, rocking(s); wag, wagging(s); asym, asymmetric; sym, symmetric; ip, in-plane; op, out-of-plane; Me, methyl; UT, unmethylated-*trans*; UC, unmethylated-*cis* and MT, methylated-*trans*.

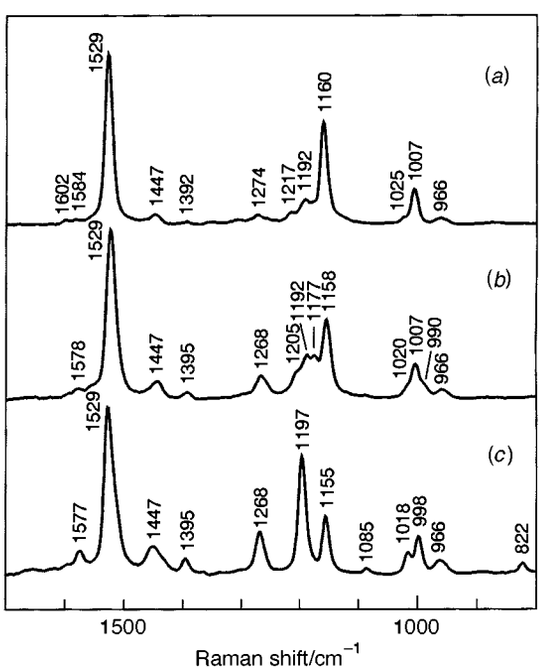

Fig. 4 Raman spectra probed at 514.5 nm of the (*a*) all-*trans*, (*b*) 11-*cis* and (*c*) 11,11′-di-*cis* isomers; in *n*-hexane, at liquid nitrogen temperature

Raman lines at 1577 and 1529 cm^{-1} can be associated with the C11=C12 (C11′=C12′), C13=C14 (C13′=C14′) and C15=C15′ stretches (based on the symmetry of this molecule, the vibrations shown in parentheses which are taking place on one side of the conjugated chain will be omitted for simplicity). More specifically, two groups of stretching vibrations, *i.e.* the C11=C12 and C15=C15′ stretches and the C13=C14 stretch, couple in-phase (out-of-phase) to give rise to the strong 1529 cm^{-1} (weak 1577 cm^{-1}) Raman line. Hereafter, this in-phase mode will be called simply the 'C=C stretching' mode. (2) The 1447 and 1395 cm^{-1} Raman lines can be assigned to the methyl asymmetric and symmetric deformations. (3) The Raman line at 1268 cm^{-1} can be assigned to the C11–H and C12–H in-plane (ip) bends which are coupled with the C11=C12 stretching; this vibrational mode has been called 'the unmethylated-*cis* (UC) mode'.[14,18] (4) A strong Raman line at 1197 cm^{-1} can be assigned to a coupled vibration consisting of the C12–C13 stretch and the C11–H and C14–H ip bends. (5) A medium Raman line at 1155 cm^{-1} can be assigned to a coupled vibration of the C14–C15 stretch, the C10–C11 stretch and the C15–H ip bend. [These pair of Raman lines, (4), (5), can be characterized as a mixture of two types of vibrations, *i.e.* one taking place around the 11-*cis* bends and the other taking place in the central all-*trans* fragment.] (6) Weak Raman lines at 1018 and 998 cm^{-1} can be assigned to the ip rockings of the 9-methyl and the 13-methyl groups, respectively. Those Raman lines due to the out-of-plane (op) vibrational modes can be resonance-enhanced when a twisting of the conjugated chain takes place.[24] (7) A very weak Raman line at 1085 cm^{-1} can be assigned to the op rocking of the 13-Me group which is strongly perturbed in the concave side of the 11-*cis* configuration. (8) A Raman line at 966 cm^{-1} can be assigned to a coupled vibration of the C11–H and C12–H op wagging and the C11=C12 torsion, which is overlapped with another coupled vibration of the C15–H and C15′–H op wagging and the C15=C15′ torsion. (9) A weak Raman line at 822 cm^{-1} can be assigned to the C11–H and C12–H op wagging. Both of the Raman lines, (7) and (9), are uniquely found in the 11,11′-di-*cis* isomer.

The assignment of the Raman lines of the 11-*cis* isomer due to the in-plane modes can be given in a similar way. Only the Raman lines unique to this mono-*cis* isomer (no symmetry) will be described below: (1′) The Raman line at 1205 cm^{-1} can be assigned to a coupled vibration consisting of the C12′–C13′ stretch and the 14′H, 15′H and 15H ip bends, whereas the Raman line at 1192 cm^{-1} can be assigned to a coupled vibration consisting of the C8′–C9′ stretch and the 10′H and 11′H bends. (2′) A pair of Raman lines at 1177 and 1158 cm^{-1} can be related to the C14–C15 and C14′–C15′ stretches; these stretches are coupled out-of-phase in the former weak Raman line and in-phase in the latter strong Raman line. (3′) The Raman lines at 1007 and 990 cm^{-1} can be assigned to the 13′Me and 13Me ip rocking, respectively.

Table 2 (the last column) compares the frequencies of the 'C=C stretching' mode, *i.e.* the in-phase coupled mode consisting of the C15=C15′, C13=C14 (C13′=C14′) and C12=C13 (C12′=C13′) stretches, which gives rise to the highest Raman intensity. It was shown that the frequency of this mode

increases systematically in the order: all-*trans*; 7-, 9-, and 13-mono-*cis*; and then di-*cis*.[18] The systematic changes can be explained in terms of a decrease in conjugation, when a *cis*-bend is introduced from the peripheral to the centre of the conjugated chain in the mono-*cis* isomers, and when an additional *cis* bend is introduced in the di-*cis* isomers. The 15-*cis* isomer does not exactly follow this rule (its frequency is lower than that of 13-*cis*), and this observation can be ascribed to the coupling of the C15=C15′ stretch with a pair of C15–H and C15′–H bends, a situation which is found uniquely in this isomer; the counterpart of this coupled vibration (the C15–H and C15′–H bends coupled with the C15=C15′ stretch) gives rise to the key Raman line of this isomer at 1247 cm^{-1}.[18]

The 'C=C stretching' frequencies of the 11-*cis* and 11,11′-di-*cis* isomers do not follow the above systematic changes at all, and they are identical to that of the all-*trans* isomer. Here again, this anomaly is ascribable to the twisting of the C11=C12 (C11′=C12′) bond, which results in a decrease in the bond order, and thus, a decrease in the stretching force constant for the particular *cis* double bond(s). On the other hand, the pair of op Raman lines which are found uniquely in the 11,11′-di-*cis* isomer, *i.e.* the C11–H and C12–H op wagging at 822 cm^{-1} and the C13 methyl op rocking at 1085 cm^{-1} suggest substantial twisting around the C11=C12 (C11′=C12′) and the C12–C13 (C12′–C13′) bonds, respectively.

Unique H and C chemical shifts of the 11-*cis* and 11,11′-di-*cis* isomers

Table 1 lists the H chemical shifts of the all-*trans*, 11-*cis*, 11,11′-di-*cis* and 15-*cis* isomers. Fig. 5(*a*) compares the chemical shifts of olefinic Hs between the 11-*cis* and the all-*trans* isomers (open and closed circles indicate the values for the 11-*cis* and the all-*trans* isomers, respectively; shaded circles are used when they are in agreement). For H nuclei, the magnetic shielding comes from the diamagnetic term due to the s electrons, and therefore, the H chemical shift can be correlated directly to the electron density[25] (we assume that the neighbouring anisotropy effects should be the same for each H nucleus in question, since they are located in a similar environment in the π conjugated system). Introduction of an 11-*cis* configuration to the extended conjugated chain of the all-*trans* isomer (see Fig. 1 for the isomeric structures) causes the hfs of the olefinic 11H and 12H due to the release of the steric interaction present in the all-*trans* configuration (release of the 11H · · · 13Me-H and 10H · · · 12H interactions), and also the lfs of the olefinic 10H and 13Me-H due to the newly introduced severe steric interaction between them. These hfs and lfs are clearly seen in Fig. 5(*a*). Fig. 5(*a*) also shows that this effect extends and decays toward the central part of the conjugated backbone. Table 1 shows that the isomerization shifts in the 13Me-H, 14H and 15H of the 11,11′-di-*cis* isomer are very different from those of the 11-*cis* isomer. These differences suggest that the symmetric introduction of the two *cis* bends causes interference of the above-mentioned extended effects coming from both sides.

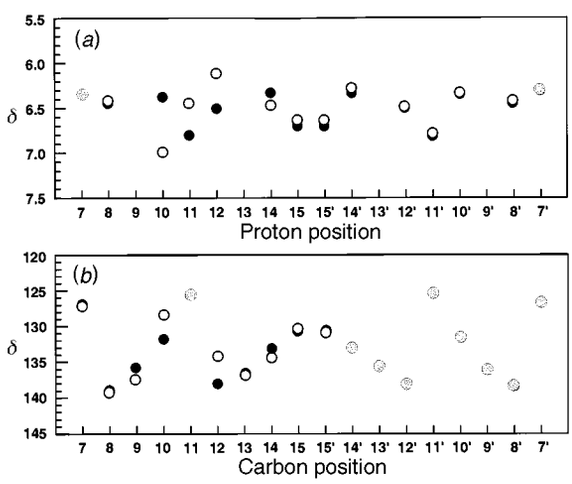

Fig. 5 Comparison of the (*a*) H and (*b*) C chemical shifts between the 11-*cis* (open circles) and the all-*trans* (closed circles) isomers; shaded circles are used when the chemical-shift values are in agreement

Fig. 6(*a*) compares the H chemical shifts of 11-*cis*-β-carotene with those of 11-*cis*-retinal and 15-*cis*-β-carotene (in the vicinity of each *cis* bend). (1) Concerning the H chemical shifts on the concave side of the *cis* bend, the signals due to 10H and 13Me-H are shifted to much lower field in 11-*cis*-β-carotene than in 11-*cis*-retinal, an observation which suggests that the steric interaction among those Hs is much more severe in the former. (2) The lfs of the olefinic 10H in 11-*cis*-β-carotene is larger than that of 15H (15′H) in 15-*cis*-β-carotene, an observation which suggests that the steric interaction in the concave side is more severe in the former than in the latter. (3) In the vicinity of the 11-*cis* bend, the 11,11′-di-*cis* isomer shows H chemical shifts similar to those of the 11-*cis* isomer (Table 1). These results lead us to the conclusion that the large lfs of the 10H and the 13Me-H signals display evidence for very severe steric interaction between the relevant Hs in both the 11-*cis* and the 11,11′-di-*cis* isomers.

For ^{13}C (hereafter abbreviated as C) nuclei, the magnetic shielding comes mainly from the paramagnetic term due to the 2p electrons rather than the diamagnetic term.[25b] The former is of opposite sign to the latter, and the absolute value is inversely proportional to the cube of the distance between a 2p electron and the nucleus. Therefore, when the electron density increases, the above distance increases due to repulsive interaction among the electrons, and then effective shielding (decrease in deshielding) takes place. Thus, the higher density of electrons causes hfs. The C chemical shift is under the influence of the carbon hybridization (the sp^2, sp and then sp^3 carbon toward the higher field), the inductive and mesomeric effects (higher electron density toward the higher field), and the steric interactions (steric perturbation on the hydrogen atom in a C–H bond

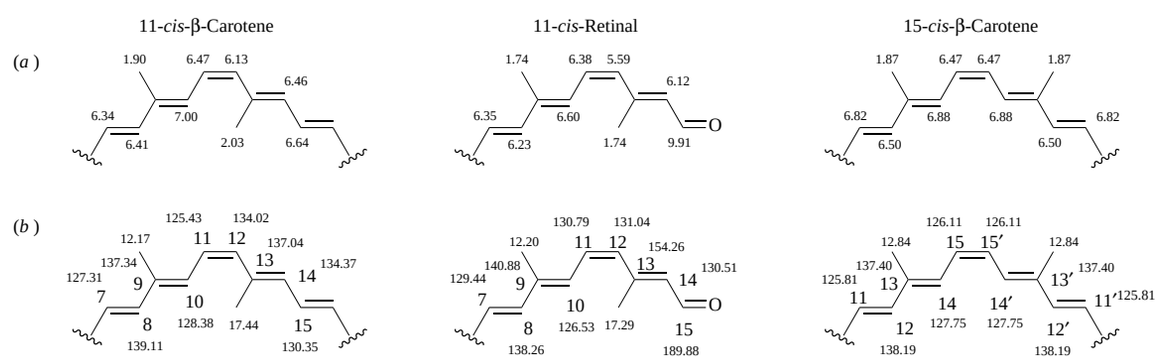

Fig. 6 Comparison of the (*a*) H and (*b*) C chemical shifts, in the vicinity of the *cis* bend, among 11-*cis*-β-carotene, 11-*cis*-retinal and 15-*cis*-β-carotene

Table 4 The C chemical shifts (isomerization shifts) of all-*trans*, 11-*cis*- and 11,11′-di-*cis*- and 15-*cis*-β-carotenes in [$^2H_6$]benzene (ppm)

Carbon	all-*trans*	11-*cis*	11,11′-di-*cis*	15-*cis*	Carbon	all-*trans*	11-*cis*	11,11′-di-*cis*	15-*cis*
1C 1′C	34.52	34.52 34.52	34.52	34.54 (+0.02)	11C 11′C	125.45	125.43 (−0.02) 125.43 (−0.02)	125.40 (−0.05)	125.81 (+0.36)
2C 2′C	39.82	39.72 (−0.10) 39.82	39.72 (−0.10)	39.81 (−0.01)	12C 12′C	138.00	134.02 (−3.98) 138.00	134.02 (−3.98)	138.19 (+0.19)
3C 3′C	19.65	19.66 (+0.01) 19.66	19.67 (+0.02)	19.67 (+0.02)	13C 13′C	136.69	137.04 (+0.35) 136.72 (+0.03)	137.05 (+0.36)	137.40 (+0.71)
4C 4′C	33.29	33.19 (−0.10) 33.29	33.19 (−0.10)	33.27 (−0.02)	14C 14′C	133.27	134.37 (+1.10) 133.23 (−0.03)	134.32 (+1.05)	127.75 (−5.52)
5C 5′C	129.37	129.30 (−0.07) 129.36 (−0.01)	129.28 (−0.09)	129.37	15C 15′C	130.63	130.35 (−0.28) 130.83 (+0.20)	130.52 (−0.11)	126.11 (−4.52)
6C 6′C	138.28	138.23 (−0.05) 138.29 (+0.01)	138.23 (−0.05)	138.28	16C 16′C	29.18	29.13 (−0.05) 29.18	29.13 (−0.05)	29.18
7C 7′C	126.80	127.31 (+0.51) 126.79 (−0.01)	127.28 (+0.48)	126.91 (+0.11)	17C 17′C	29.18	29.13 (−0.05) 29.18	29.13 (−0.05)	29.18
8C 8′C	138.69	139.11 (+0.42) 138.70 (+0.01)	139.12 (+0.43)	138.75 (+0.06)	18C 18′C	22.05	21.97 (−0.08) 22.05 (−0.65)	21.97 (−0.08)	22.04 (−0.01)
9C 9′C	135.95	137.34 (+1.39) 135.93 (−0.02)	137.28 (+1.33)	136.15 (+0.20)	19C 19′C	12.82	12.17 (−0.65) 12.82	12.16 (−0.66)	12.84 (+0.02)
10C 10′C	131.95	128.38 (−3.57) 131.94 (−0.01)	128.36 (−3.59)	131.83 (−0.12)	20C 20′C	12.85	17.44 (+4.59) 12.82 (−0.03)	17.41 (+4.56)	12.56 (−0.29)

causes the shift of electrons from H to C, and thus, the hfs of the C signal).[25b]

Table 4 lists the C chemical shifts of the all-*trans*, 11-*cis*, 11,11′-di-*cis* and 15-*cis* isomers of β-carotene, and Fig. 5(*b*) compares the chemical shifts of the olefinic carbons between the 11-*cis* and the all-*trans* isomers. Introduction of an 11-*cis* configuration causes changes in the C chemical shifts due to electronic redistribution on the carbon atoms as a result of the electron-density changes on the hydrogen atoms due to steric interactions. Specifically, the isomerization shift of 10C is in the opposite direction to that of 10H, an observation which shows that electrons are pushed from 10H to 10C due to the severe steric interaction applied to 10H. However, the isomerization shift of 12C in the same direction as that of 12H as well as the very small isomerization shift of 11C despite the large isomerization shift of 11H suggest the presence of another effect causing the hfs of both 11C and 12C; this is most probably the effect of twisting around the C11=C12 bond which causes a change in hybridization of the pair of carbon atoms from the sp^2-type to the sp^3-type. These effects of electronic redistribution and hybridization extend to both 7C in the peripheral and to 15′C in the centre of the conjugated chain. Introduction of a pair of 11-*cis* configurations in the 11,11′-di-*cis* isomer causes very similar changes in the C chemical shift except for 15C (see Table 4). Here again, symmetric introduction of the two 11-*cis* bends seems to cause interference of this effect at the centre of the conjugated chain.

Fig. 6(*b*) compares the C chemical shifts of 11-*cis*-β-carotene with those of 11-*cis*-retinal and 15-*cis*-β-carotene. Concerning the *cis* double bond, larger differences in chemical shift between the 11C and 12C are seen in 11-*cis*-β-carotene than in 11-*cis*-retinal. The result suggests that polarization of the 11C=12C bond takes place in the case of 11-*cis*-β-carotene. When a pair of resonance structures, 11C=12C ⟷ $11C^-$–$12C^+$, is assumed, the above chemical-shift difference indicates that the contribution of the latter resonance structure is enhanced in 11-*cis*-β-carotene. This polarization suggests the contribution of the zwitterionic state, and therefore, a twisting around the C11=C12 double bond.[26] In retinal, this polarization is most probably compensated for by the electron-withdrawing inductive effect of the terminal carbonyl group.[13] In 15-*cis*-β-carotene, no polarization is expected for the C15=C15′ bond because of the C_{2v} (or C_2) symmetry of the molecule.

Thermal isomerization starting from the 11-*cis* and 11,11′-di-*cis* isomers

Fig. 7 compares time-dependent changes in the isomeric composition in thermal isomerization at 38 °C starting from the (*a*) 11-*cis*, (*b*) 11,11′-di-*cis* and (*c*) 15-*cis* isomers. The 15-*cis* isomer was chosen for comparison, because it was thermally the least stable isomer previously known.[20] Fig. 7(*a*) shows that the 11-*cis* isomer mainly isomerizes into the all-*trans* isomer (minor products, less than 2%, are not shown). Fig. 7(*b*) shows that the 11,11′-di-*cis* isomer isomerizes into the 11-*cis* isomer, and then, the resultant 11-*cis* isomer isomerizes into the all-*trans* isomer. The fitting curves in both figures are based on a pair of sequential first-order reactions [eqns. (1) and (2)], where the

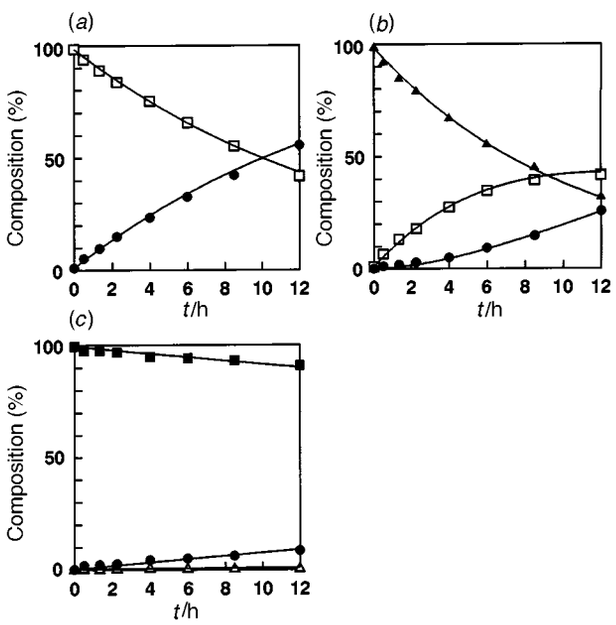

Fig. 7 Time-dependent changes in the isomeric composition in the thermal isomerization at 38 °C starting from the (*a*) 11-*cis*, (*b*) 11,11′-di-*cis* and (*c*) 15-*cis* isomers; open square (11-*cis*), closed circle (all-*trans*), closed triangle (11,11′-di-*cis*), closed square (15-*cis*) and open triangle (13-*cis*)

$$11\text{-}cis \xrightarrow{k_{11\longrightarrow t}} \text{all-}trans \qquad (1)$$

$$11,11'\text{-di-}cis \xrightarrow{k_{11,11'\longrightarrow 11}} 11\text{-}cis \qquad (2)$$

values of $k_{11\longrightarrow t}$ and $k_{11,11'\longrightarrow 11}$ were determined (at 38 °C) to be 18.9×10^{-6} and 26.3×10^{-1} s^{-1}, respectively (see Table 5). Agreement between the fitting curves and the observed points is

Table 5 The rate constant, the frequency factor and the activation energy of each thermal-isomerization pathway

		11-*cis* ⟶ all-*trans*	11,11′-di-*cis* ⟶ 11-*cis*	15-*cis* ⟶ all-*trans*	15-*cis* ⟶ 13-*cis*	13-*cis* ⟶ all-*trans*
Rate constant/10^6 s^{-1}	28 °C	5.09 ± 0.13	6.29 ± 0.15	0.72 ± 0.04	0.16 ± 0.04	0.46[a]
	38 °C	18.9 ± 0.02	26.3 ± 0.03	2.11 ± 0.11	0.18 ± 0.11	1.88[a]
	48.5 °C	61.7 ± 1.92	94.5 ± 2.14	6.61 ± 0.19	0.58 ± 0.20	7.50[a]
Frequency factor/s^{-1}		$(5.16 \pm 7.17) \times 10^{11}$	$(1.85 \pm 2.83) \times 10^{13}$	$(8.93 \pm 2.95) \times 10^{8}$	$(0.76 \pm 4.10) \times 10^{2}$	4.75×10^{12}
Activation energy/ kcal mol^{-1}		23.4 ± 0.9	25.4 ± 0.9	20.8 ± 0.2	12.1 ± 3.3	26.2

[a] Ref. 21.

quite satisfactory, a fact which indicates that the above first-order isomerization reactions predominate.

Fig. 7(*c*) shows that the 15-*cis* isomer isomerizes into both the all-*trans* and the 13-*cis* isomers as reported previously.[20] The fitting curves are based on a pair of parallel first-order reactions [eqns. (3) and (4)], where the values of $k_{15 \longrightarrow t}$ and $k_{15 \longrightarrow 13}$ were

$$15\text{-}cis \xrightarrow{k_{15 \longrightarrow t}} \text{all-}trans \quad (3)$$

$$15\text{-}cis \xrightarrow{k_{15 \longrightarrow 13}} 13\text{-}cis \quad (4)$$

determined to be 2.11×10^{-6} and 0.18×10^{-6} s^{-1}, respectively.

The above results indicate that the value of $k_{11 \longrightarrow t}$ is 9.0 times larger than that of $k_{15 \longrightarrow t}$ and that the $k_{11,11' \longrightarrow 11'}$ value is 1.4 times larger than the $k_{11' \longrightarrow t}$ value. Therefore, the relative stability of the isomers which is defined as a decrease in the starting isomer is in the order, 15-*cis* > 11-*cis* > 11,11′-di-*cis*. Thus, together with the results of thermal isomerization from the all-*trans*, 7-*cis*, 9-*cis*, 13-*cis* and 15-*cis* isomers,[20] the relative stability among the all-*trans* and mono-*cis* isomers is now determined to be in the order: all-*trans* > 7-*cis* > 9-*cis* > 13-*cis* > 15-*cis* > 11-*cis*.

Concerning the isomerization pathways, we characterized thermal isomerization starting from the all-*trans*, 7-*cis*, 9-*cis*, 13-*cis* and 15-*cis* isomers in terms of three different types of isomerizations, *i.e.* '*cis*-to-*trans*' isomerization, '*trans*-to-*cis*' isomerization, and '*cis*-to-*cis*' isomerization.[20] (1) The all-*trans* isomer and the 7-*cis* (a peripheral-*cis*) isomer were characterized by '*trans*-to-*cis*' isomerization preferably in the central part: all-*trans* ⟶ 13-*cis*, 15-*cis* and 9-*cis*; and 7-*cis* ⟶ 7,13′-di-*cis*, 7,15-di-*cis* and 7,13-di-*cis*. (2) The 9-*cis* isomer was characterized by both '*trans*-to-*cis*' and '*cis*-to-*trans*' isomerization in a similar magnitude: 9-*cis* ⟶ 9,13′-di-*cis*, 9,15-di-*cis*, 9,13-di-*cis* and all-*trans*. (3) The 13-*cis* isomer was characterized by major '*cis*-to-*trans*' isomerization (13-*cis* ⟶ all-*trans*) and minor '*cis*-to-*cis*' isomerization (13-*cis* ⟶ 15-*cis*). (4) The 15-*cis* isomer was characterized by major '*cis*-to-*trans*' isomerization (15-*cis* ⟶ all-*trans*) and by minor but much more pronounced '*cis*-to-*cis*' isomerization (15-*cis* ⟶ 13-*cis*). Based on all the above results, it is concluded that the uniqueness of the 11-*cis* and 11,11′-di-*cis* isomers lies in the major '*cis*-to-*trans*' isomerization.

Table 5 lists the rate constant, the frequency factor and the activation energy for each isomerization pathway, which were determined by thermal isomerization at 28, 38 and 48.5 °C. The rate constants ($k_{11 \longrightarrow t}$ and $k_{11,11' \longrightarrow 11}$) at 28 and 38 °C were determined by non-linear least-squares fitting to all the observed points, but those at 48.5 °C were determined by the use of data points until 5.5 h of thermal isomerization because analysis by assuming the first-order reactions became difficult. For the determination of the $k_{15 \longrightarrow t}$ and $k_{15 \longrightarrow 13}$ values, all the data points and the $k_{13 \longrightarrow t}$ value which was calculated based on Doering *et al.*[21] were used.

The frequency factor for the 11,11′-di-*cis* to 11-*cis* isomerization is of the order of 10^{-13}, a value which is expected for a complete adiabatic process;[27] the frequency factors for the isomerizations from 13-*cis*, 11-*cis* and 15-*cis* to all-*trans* are one, two and five orders of magnitude lower. On the other hand, the activation energies which were determined for the *cis*-to-*trans* isomerization are in the order, 11,11′-di-*cis* to 11-*cis* > 11-*cis* to all-*trans* > 15-*cis* to all-*trans*. This order is in contrast to the order of the rate constants, $k_{11,11' \longrightarrow 11} > k_{11 \longrightarrow t} > k_{15 \longrightarrow t}$. Therefore, each *cis* to *trans* isomerization cannot be explained simply in terms of an adiabatic potential curve around the relevant carbon–carbon double bond. Further investigation is necessary to reveal the isomerization mechanism for each pathway.

The structures of the 11-*cis* and 11,11′-di-*cis* isomers predicted by molecular force-field calculations

Table 6 compares the bond lengths, the bond angles and the dihedral angles of the all-*trans*, 7-*cis*, 9-*cis*, 11-*cis*, 13-*cis*, 15-*cis* and 11,11′-di-*cis* isomers which have been optimized by molecular-mechanics (MM2) calculations (the values for the one-half of the conjugated skeleton are shown). This is basically a molecular force-field calculation (see Experimental) in which the nuclei and the electrons in each atom are lumped together as a particle. We have tried to obtain information concerning the effects of molecular strain on the geometry of each isomer.

The molecular force-field calculation predicts that the 11-*cis* configuration releases the severe steric repulsion between the 13Me-H and the olefinic 10H by a large increase in one of the bond angles in the *cis* bend, by twisting around the *cis* double bond, and by twisting around the neighbouring pair of single bonds. In the 11-*cis* (11,11′-di-*cis*) isomer, the C11=C12–C13 bond angle is predicted to be 128.7° (128.3°) and the dihedral angles around the C10–C11, C11=C12 and C12–C13 bonds to the 172.3, −8.8 and 156.1° (173.7, −8.8 and 153.3°), respectively. In the case of the 15-*cis* isomer, no such distortion is found in the vicinity of the *cis* bend: The C14–C15=C15′ bond angle is not very large (126.6°), and the torsional angles around the C14–C15 and C15=C15′ bonds indicate complete *trans* (179.7°) and *cis* (0.0°) configurations.

Concerning the structure of the 11,11′-di-*cis* isomer, the molecular force-field calculation predicts that the planar C_{2h} structure is unstable, and that a pair of structures, which we call the 'C_2 structure' and the 'C_i structure', are more stable and have the same strain energy. Fig. 8 shows these two structures; the top views, (*a*) and (*c*), show that the former is in a curled form and that the latter is in a pleated-sheet form. The steric energies of the all-*trans*, 15-*cis*, 11-*cis* and 11,11′-di-*cis* isomers were calculated to be 16.7, 19.6, 21.6 and 26.0 kcal mol^{-1}.

Now we try to correlate the unique properties of the 11-*cis* and the 11,11′-di-*cis* isomers experimentally determined with the results of molecular force-field calculations. (*a*) The wavelengths of the $B_u^+ \leftarrow A_g^-$ absorption in the 11-*cis* and the 11,11′-di-*cis* isomers, which are similar to that of the all-*trans* isomer and do not follow the systematic blue-shift found in other mono-*cis* and di-*cis* isomers, can be explained in terms of the predicted twisting around both the double (C11=C12) and the single (C12–C13) bonds. The PPP-CI calculations on the model polyene (*vide supra*) predicted that the twisting

Table 6 The bond lengths, bond angles, dihedral angles and steric energy of each isomer predicted by the MM2 calculations

Atom position	6	7	8	9	10	11	12	13	14	15	15′
⟨all-*trans*, 16.7 kcal mol^{-1}⟩											
Bond length	1.489[a]	1.350	1.475	1.360	1.466	1.356	1.474	1.361	1.465	1.356	
Bond angle		122.5[b]	125.4	117.2	125.2	121.6	125.1	117.3	125.2	121.8	121.8
Dihedral angle	−125.8[c]	177.9[d]	167.5	−179.4	178.7	−180.0	166.5	−179.5	178.8	179.7	
⟨7-*cis*, 19.0 kcal mol^{-1}⟩											
Bond length	1.488	1.349	1.478	1.358	1.466	1.356	1.473	1.361	1.465	1.356	
Bond angle		126.8	127.7	117.2	124.7	121.8	125.4	117.3	125.4	121.8	121.8
Dihedral angle	−127.4	5.0	−154.6	179.0	−178.5	179.7	171.4	−178.7	−177.7	179.1	
⟨9-*cis*, 17.3 kcal mol^{-1}⟩											
Bond length	1.490	1.349	1.472	1.361	1.464	1.358	1.472	1.363	1.464	1.358	
Bond angle		122.7	124.0	121.9	126.7	121.8	124.6	117.2	126.7	121.7	121.7
Dihedral angle	−128.8	179.6	164.7	−3.6	−176.3	178.3	179.5	−179.7	−175.7	178.4	
⟨11-*cis*, 21.6 kcal mol^{-1}⟩											
Bond length	1.489	1.351	1.474	1.362	1.465	1.355	1.477	1.359	1.464	1.357	
Bond angle		123.0	125.2	117.2	125.0	126.7	128.7	117.2	125.2	121.9	121.9
Dihedral angle	−128.5	179.7	162.5	−179.0	172.3	−8.8	156.1	177.5	−177.2	179.2	
⟨13-*cis*, 17.3 kcal mol^{-1}⟩											
Bond length	1.490	1.350	1.475	1.360	1.466	1.357	1.471	1.361	1.465	1.358	
Bond angle		122.2	125.1	117.3	125.0	122.0	123.9	122.3	127.6	121.3	122.2
Dihedral angle	−123.0	179.3	166.8	−178.2	178.8	−179.4	174.8	−1.4	179.2	−178.5	
⟨15-*cis*, 19.6 kcal mol^{-1}⟩											
Bond length	1.489	1.351	1.474	1.361	1.465	1.357	1.473	1.363	1.464	1.358	
Bond angle		122.8	125.0	117.4	124.9	122.2	124.7	117.7	124.5	126.6	126.6
Dihedral angle	−125.9	178.1	167.4	−178.5	179.3	−178.9	166.0	−177.5	179.7	0.0	
⟨11,11′-di-*cis*, C_i, 26.0 kcal mol^{-1}⟩											
Bond length	1.489	1.350	1.475	1.361	1.465	1.355	1.478	1.359	1.467	1.356	
Bond angle		122.7	125.4	117.1	125.2	126.4	128.3	117.2	125.0	121.8	121.8
Dihedral angle	−127.5	180.0	163.7	−178.9	173.7	−8.3	153.3	178.9	−179.1	−180.0	
⟨11,11′-di-*cis*, C_2, 26.0 kcal mol^{-1}⟩											
Bond length	1.489	1.350	1.474	1.360	1.465	1.355	1.477	1.359	1.466	1.465	
Bond angle		122.4	125.6	116.9	125.3	126.0	128.1	117.3	124.9	121.8	121.8
Dihedral angle	−126.5	180.0	164.8	−178.5	173.9	−8.0	151.9	179.0	−178.3	−179.5	

Each bond length, bond angle and dihedral angle are to be read as follows: [a] The C6–C7 bond length, [b] the C6–C7–C8 bond angle, [c] the C1–C6–C7–C8 dihedral angle and [d] the C6–C7–C8–C9 dihedral angle.

around the double bond (single bond) is expected to cause a red (blue) shift. Therefore, these effects in the opposite direction and the additional effect of introducing a *cis* bend in the conjugated chain are assumed to result in such similar wavelengths. (*b*) The small ε value in the 11-*cis* isomer and the extremely small ε value in the 11,11′-di-*cis* isomer can be explained in terms of the predicted structures, because the PPP-CI calculations of the model polyene (*vide supra*) predicted a decrease in oscillator strength upon twisting around the C11=C12 and/or the C12–C13 (C10–C11) bonds. Further, the molecular force-field calculation predicts that introduction of one and then two 11-*cis* configuration(s) should cause a twisted and curled structure of the entire conjugated chain (see Fig. 8) and, as a result, a shortening of the end-to-end distance; this structural distortion must cause a decrease in their oscillator strengths. (*c*) The observation of the *cis* peak ($A_g^+ \leftarrow A_g^-$ absorption) in the 11,11′-di-*cis* isomer strongly supports its C_2 structure, because this transition is forbidden in the C_i structure. The PPP-CI calculations of the model polyene (*vide supra*) suggested that the $A_g^+ \leftarrow A_g^-$ absorption is strongly enhanced upon twisting around the C12–C13 and the C11=C12 bonds. Further, the end-to-end distance of the conjugated chain is shorter in the C_2 structure than in the C_i structure (Fig. 8), leading to a decrease in the $B_u^+ \leftarrow A_g^-$ absorption in the former due to the curled structure. The combination of these two effects must cause the extremely high relative intensity of the $A_g^+ \leftarrow A_g^-$/$B_u^+ \leftarrow A_g^-$ absorptions for this di-*cis* isomer. (*d*) The 'C=C stretching' frequencies of the 11-*cis* and 11,11′-di-*cis* isomers, which are identical to that of the all-*trans* isomer and do not follow the systematic high-frequency shifts in other mono-*cis* and di-*cis* isomers, can be explained in terms of the predicted twisting around the *cis* C11=C12 double bond. This twisting must cause a decrease in the C=C stretching force constant. (*e*) The appearance of the Raman lines due to the out-of-plane vibrations in the 11,11′-di-*cis* isomer can be explained in terms of the twisting of the conjugated chain around the C12–C13 (C12′–C13′) and C11=C12 (C11′=C12′) bonds. (*f*) The severe steric strain evidenced by the large lfs of the 13Me-H and 10H NMR signals in both the 11-*cis* and 11,11′-di-*cis* isomers can be released by the predicted changes in the dihedral angles around the C10–C11, C11=C12 and C12–C13 bonds. (*g*) The chemical shifts of C11 and C12, both of which appear at much higher field than expected, can be explained in terms of a change in hybridization from the sp^2-type to the sp^3-type which is caused by the predicted twisting around the *cis* C11=C12 bond. The electronic polarization of these carbon atoms which was identified by differences in the C chemical shifts can also be explained by this twisting. (*h*) The predicted strain energy in the order, all-*trans* < 15-*cis* < 11-*cis* < 11,11′-di-*cis*, agrees with the observed relative instability. (Concerning the 7-*cis*, 9-*cis* and 13-*cis* isomers, the order of the strain energy does not agree with the observed relative stability, *vide supra*.)

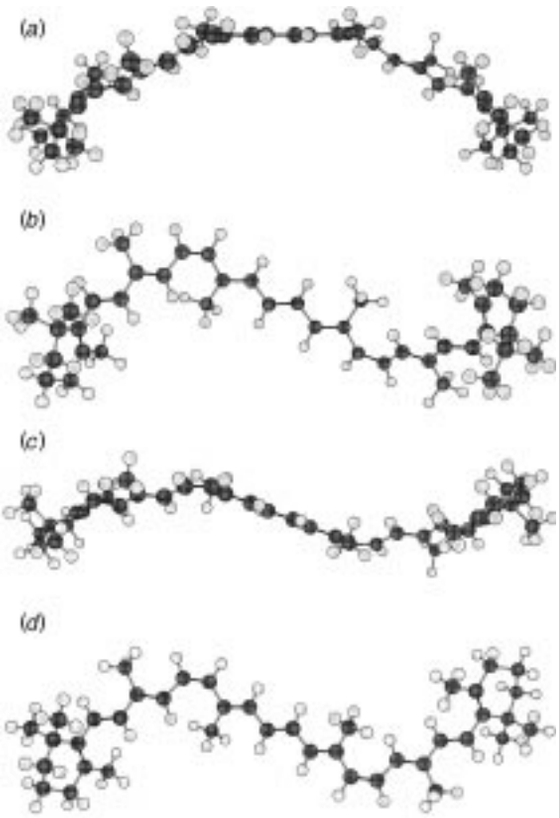

Fig. 8 Two different structures of the 11,11′-di-*cis* isomer predicted by the MM2 calculations. (*a*) The top view and (*b*) the front view of the 'C_2 structure', and (*c*) the top view and (*d*) the front view of the 'C_i structure'. The electronic absorption data support the 'C_2 structure'.

Structural strain and inherent instability: why the 11-*cis* configuration has not been found in the natural carotenoids

The structural strain due to the severe steric interaction between the 13Me-H and the olefinic 10H in the concave side of the 11-*cis* bend is now evidenced. All the experimental data of electronic-absorption, resonance-Raman and ^{1}H and ^{13}C NMR spectroscopy as well as the molecular force-field and the PPP-CI calculations indicate that this structural strain must be partially released by twisting around the *cis* double bond and particularly around one of the neighbouring single bonds. The 11-*cis* isomer is suggested to take a twisted structure, whereas the 11,11′-di-*cis* isomer takes a curled structure of C_2 symmetry.

Analyses by HPLC of the purified 11-*cis* and 11,11′-di-*cis* isomers showed that these isomers are stable enough to be isolated, but analysis of their thermal isomerization identified a very efficient isomerization pathway of 11,11′-di-*cis*→11-*cis* ⟶ all-*trans* even at room temperature. There has been no direct evidence for thermal isomerization from all-*trans* to 11-*cis*.[20] Therefore, the 11-*cis* configuration is destined to disappear thermally, although it can be produced synthetically. The 11-*cis* and the 11,11′-di-*cis* isomers are the least stable isomers among all the *cis–trans* isomers of β-carotene which have ever been examined.

Concerning the usage of the *cis* carotenoids in the photosynthetic reaction centres (RCs), the most conspicuous difference between the 15-*cis* and the 11-*cis* isomers must lie in the former being thermally much more stable than the latter (in the case of β-carotene, almost one order of magnitude in terms of isomerization rate). Actually, 15-*cis*-β-carotene can be produced by thermal isomerization from all-*trans*-β-carotene in solution.[20] Further, 15-*cis*-spheroidene can be produced when all-*trans*-spheroidene is bound to the RC which is obtained from a 'carotenoid-less' mutant of *Rhb. sphaeroides*.[28] The 15-*cis* configuration must be more useful for the RCs to perform the photo-protective function, because it can be generated thermally through intermolecular interaction with the apo-peptide.

The structural strain due to the severe steric hindrance and the resultant thermal instability must be the main reason why the 11-*cis* configuration has not been found in the natural carotenoids. Most probably, the 11-*cis* carotenoids are too unstable to be used for any physiological function.

Experimental

Synthesis of 11-*cis* and 11,11′-di-*cis*-β-carotenes

Scheme 1 shows the steps to synthesize the 11-*cis* and 11,11′-di-*cis* isomers of β-carotene. They were prepared from the corresponding acetylenic C_{40}-precursors **3** and **6** by semihydrogenation of the triple bond(s) over Lindlar catalyst to selectively form the *cis*-configurated double bond(s). 11,12-Didehydroretinal[29] **1**, readily available from known 11,12-didehydroretinol,[29a,c,30] was used as a common intermediate. Wittig condensation of 11,12-didehydroretinal **1** with retinyl(triphenyl)-phosphonium bromide[31] **2** provided 11,12-didehydro-β-carotene **3**. By analogy, Wittig reaction of **1** with 11,12-didehydroretinyl(triphenyl)phosphonium bromide **5**, obtained

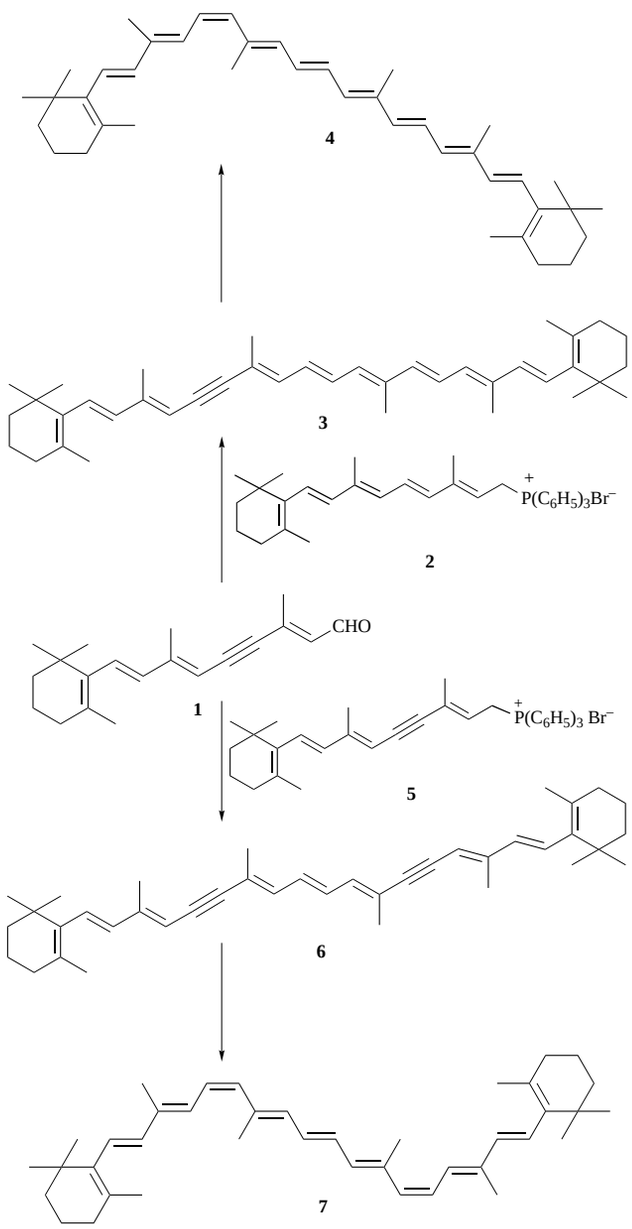

Scheme 1

from 11,12-didehydroretinol *via* the corresponding bromide, provided 11,12,11′-12′-tetrahydro-β-carotene[32] **6**. Catalytic semihydrogenation of **3** and **6** gave **4**[33] and **7**,[32] respectively. Detailed preparative procedures will be described below.

Intermediates **3**, **5** and **6** were characterized at Hoffmann-La Roche, Basel. Mass spectra were obtained on an MS 9 (AEI, GB-Manchester) spectrometer at 70 eV. Data are given as *m*/*z* (%). UV spectra (in hexane containing 2% chloroform) were recorded on a Uvikon 810 instrument; each result is shown as λ_{max} in nm (10^{-3} × molar extinction coefficient at the maximum). ^{1}H NMR spectra were recorded in $CDCl_3$ on a Bruker AC-250 at 250 MHz or a Bruker AM-400 spectrometer at 400 MHz. *J* values are in Hz.

11,12-Didehydro-β-carotene 3. To a solution of 11,12-didehydroretinal[29] **1** (4.32 g, 15.3 mmol) and retinyl(triphenyl)-phosphonium bromide[31] **2** (9.08 g, 14.9 mmol) in 35 ml of isopropyl alcohol under argon and at −25 °C were slowly added 8.7 ml of a 10% solution of potassium hydroxide in isopropyl alcohol. After stirring for 30 min, the precipitate was isolated by filtration and dried under vacuum at room temp. The orange solid was then dissolved in refluxing hexane and the triphenylphosphine oxide eliminated by filtration. The solvent was evaporated and the residue triturated in cold hexane to yield 3.6 g of crude 11,12-didehydro-β-carotene **3**. Several recrystallizations from ethyl acetate–hexane 1:1 gave 1.03 g (13%) of **3** as a red solid, mp 135–136 °C (Calc. for $C_{40}H_{54}$: C, 89.82; H, 10.18%. Found: C, 89.38; H, 10.34%); MS *m*/*z* 534 (M^+, 54%), 519 (4%), 69 (100%); λ/nm 272 (18.8), 434 (113); δ_H 6.58–6.7 (2H, m, 11′, 14H), 6.5–6.52 (2H, m, 15,15′H), 6.35 (1H, d, *J* 15, 12′H), 6.25 (1H, d, *J* 17.5, 7H), 6.22 (1H, d, *J* 12.2, 14′H), 6.18 (1H, d, *J* 15.7, 7′H), 6.15 (1H, d, *J* 12.3, 10′H), 6.13 (2H, d, *J* 16, 8,8′H), 5.59 (1H, s, 10H), 2.07 (3H, s), 2–2.05 (4H, m, 4,4′H), 1.99 (3H, s), 1.97 (6H, s), 1.72 and 1.7 (6H, 2s, 5,5′Me), 1.65–1.57 (4H, m, 3,3′H), 1.48–1.44 (4H, m, 2,2′H), 1.03 and 1.02 (12H, 2s, 1,1′Me).

11-*cis*-β-Carotene 4. To a solution of 11,12-didehydro-β-carotene **3** (0.5 g, 0.9 mmol) in 25 ml of dry tetrahydrofuran (THF) were added 0.5 g of Lindlar catalyst and 0.25 g of sodium carbonate. The reaction mixture was hydrogenated at −15 °C and at 1 atm for 6 h and then filtered over aluminium oxide. The concentration of the solvent under vacuum at 20 °C gave 417 mg crude material containing 9% **3**, 13% all-*trans*-β-carotene and 76% 11-*cis*-β-carotene[33] **4**. It was purified by preparative HPLC (*vide infra*).

all-*trans*-[3,7-Dimethyl-9-(2,6,6-trimethylcyclohex-1-enyl)nona-2,6,8-trien-4-ynyl]triphenylphosphonium bromide 5. A solution of 11,12-didehydroretinol,[29a,c,30] (14.22 g, 50 mmol) in 190 ml of ethyl acetate was treated at −20 °C with phosphorus tribromide (5.42 g, 20 mmol) in 50 ml of ethyl acetate. The reaction mixture was stirred for 1 h and ice–water (250 ml) was then cautiously poured into the reaction mixture. The organic phase was separated and the water phase again extracted with 100 ml of ethyl acetate. The organic phases were combined, washed with saturated sodium hydrogen carbonate and brine, and dried over anhydrous sodium sulfate. Triphenylphosphine (14.7 g, 56 mmol) was added to the filtered solution which was stirred overnight at room temp. The solvent was evaporated and 120 ml of acetone–diethyl ether 1:1 added to the orange residue. The mixture was then stored at 0 °C and the precipitate filtered, washed with cold diethyl ether and dried under vacuum to yield crude phosphonium salt **5**. Recrystallization from acetone–diethyl ether gave 10.5 g (34.5%) of **5** as a yellow powder, mp 128–133 °C (decomp.); MS *m*/*z* 529 (M^+, 100%); δ_H 7.7–7.95 (15H, m, arom.), 6.27 (1H, d, *J* 16), 6.1 (1H, d, *J* 16), 5.71 (1H, dd, *J* 8), 5.45 (1H, s), 4.95 (2H, dd, *J* 8), 2.01 (2H, m), 1.99 (3H, s), 1.68 (3H, s), 1.6 (2H, m), 1.58 (3H, s), 1.47 (2H, m), 1.0 (6H, s).

11,12,11′,12′-Tetradehydro-β-carotene 6. To a solution of 11,12-didehydroretinal[29] **1** (1.41 g, 5 mmol) and 11,12-didehydroretinyl(triphenyl)phosphonium bromide **5** (3.05 g, 5 mmol) in 50 ml of dichloromethane under argon and −25 °C was slowly added 0.94 ml of a 30% solution of sodium methoxide in methanol. After 30 min stirring, the solvents were evaporated and the residue partitioned between a 1:1 mixture of hexane–ethyl acetate 4:1 and methanol–water 4:1. The hexane–ethyl acetate phase was separated, dried over sodium sulfate and concentrated under vacuum. The oily residue (2.6 g) was purified by column chromatography over silica gel to yield 1.34 g of crude 11,12,11′,12′-tetradehydro-β-carotene **6**. Recrystallization from hexane gave 278 mg (10.4%) of **6** as an orange solid, mp 122–125 °C (lit.,[32] 98–100 °C) (Calc. for $C_{40}H_{52}$: C, 90.16; H, 9.84%. Found: C, 89.75; H, 9.81%); MS *m*/*z* 532 (M^+, 80%), 517 (22%), 69 (100%); λ/nm 271 (21.7), 417 (93.3); δ_H 6.50–6.53 (4H, m, 14,14′,15,15′H), 6.26 (2H, d, *J* 16, 7,7′H), 6.13 (2H, d, *J* 16, 8,8′H), 5.58 (2H, s, 10,10′H), 2.07 (6H, s, 9,9′Me), 2.01 (4H, t, *J* 6, 4,4′H), 1.99 (6H, s, 13,13′Me), 1.7 (6H, s, 5,5′Me), 1.61 (4H, m, 3,3′H), 1.46 (4H, m, 2,2′H), 1.02 (12H, s, 1,1′Me).

11,11′-di-*cis*-β-Carotene 7. To a solution of 11,12,11′,12′-tetradehydro-β-carotene **6** (1 g, 1.88 mmol) in 50 ml of dry ethyl acetate were added 0.78 g of Lindlar catalyst and 80 μl of quinoline. The reaction mixture was hydrogenated for 1 h at room temp. and 1 atm, then filtered over aluminium oxide and the solvent evaporated under vacuum at 20 °C. The oil obtained was dissolved in 10 ml dichloromethane and methanol was added until precipitation of a dark red solid which was removed by filtration. Two crystallizations from dichloromethane–methanol 1:1 gave 442 mg of crude material containing 3.5% all-*trans*-β-carotene, 6% unknown isomer and 86% 11,11′-di-*cis*-β-carotene[32] **7**.

Purification of 11-*cis* and 11,11′-di-*cis*-β-carotenes. Both the 11-*cis* and 11,11′-di-*cis* isomers as obtained with purities of 76 and 86% were then purified by HPLC using a Shimadzu LC-10AS chromatograph and a Waters 996 photodiode-array detector under the following conditions: column, a 4 mm i.d. × 300 mm column packed with calcium hydroxide at 300 kg cm^{-2} (Nacalai Tesque Inc., Lot. M5M2325); eluent, 0.5% acetone in *n*-hexane; flow rate, 0.5 ml min^{-1}; and detection, 450 nm. An 8 mm i.d. column and higher flow rate of 1.5–3.0 ml min^{-1} were used for collection and for tracing thermal isomerization of these isomers (*vide infra*).

Electronic absorption and Raman measurements

The electronic absorption spectra of isomeric β-carotene were recorded at room temp. in *n*-hexane solution on a Hitachi U-2000 spectrophotometer. The extinction coefficients were determined by the use of *ca.* 13.5–21.8 mg of isomeric β-carotene (all-*trans*, 15-*cis*, 11-*cis* and 11,11′-di-*cis*) in *n*-hexane; the mass of each sample was measured to an accuracy of 0.1 mg and then the electronic absorption at the maximum of the $B_u^+ \leftarrow A_g^-$ absorption was determined after dissolving into, and diluting with, *n*-hexane (0.3% of THF was used in the case of the all-*trans* isomer for dissolving the crystals).

The Raman spectra of isomeric β-carotene were recorded at liquid nitrogen temperature in *n*-hexane solution under a preresonance condition (see Fig. 3) by the use of the 514.5 nm line (1 mW) of a Lexel 95 Ar^+-ion laser and a JASCO TRS-300 Raman spectrometer which was equipped with a Princeton Instruments IRY-700 detector.

NMR measurements

The ^{1}H and ^{13}C NMR spectra of isomeric β-carotene were recorded at 8 °C in [$^2H_6$]benzene (CEA 99.6%) on a JEOL JNM-A400 FT NMR spectrometer. The sample concentrations were *ca.* 7.0×10^{-4}–4.7×10^{-3} and *ca.* 1.2–1.6×10^{-2} M for ^{1}H and ^{13}C NMR measurements, respectively. (1) ^{1}H NMR: The digital resolution of each 1D spectrum was 0.24 Hz. The pulse sequences for 2D measurements were as follows: ^{1}H,^{1}H-COSY, 90°–t_1–90°–t_2; long-range ^{1}H,^{1}H-COSY, 90°–t_1–90°–Δ–t_2 with $\Delta = 400$ ms; and ^{1}H,^{1}H-ROESY, 90°–t_1–τ_m–(spin-rock)–t_2,

τ_m = 250 ms. (2) ^{13}C NMR: The digital resolution of each 1D spectrum was 0.83 Hz. The pulse sequences for 2D measurements were as follows: ^{13}C,^{1}H-COSY, 90°[^{1}H]–t_1/2–180°[^{13}C]–t_1/2–Δ_1–90°[^{1}H], 90°[^{13}H]–Δ_2; ^{13}C,^{1}H-COLOC, 90°[^{1}H]–t_1/2–180°[^{1}H], 180°[^{13}C]–{Δ_1–t_1/2}–90°[^{1}H], 90°[^{13}C]–Δ_2; ^{13}C,^{1}H-DEPT, 90°[^{1}H]–τ–180°[^{1}H], 90°[^{13}C]–τ–θ_y[^{1}H], 180°[^{13}C]–τ (θ_y = 45°, 90° and 135°).

Thermal isomerization

Thermal isomerization of the 11-*cis*, 11,11′-di-*cis* and 15-*cis* isomers was traced by HPLC at 28, 38 and 48.5 °C. Each isomer in a 0.5% acetone in *n*-hexane solution (concentrations, *ca.* 1.6–2.3 × 10^{-5} M) immediately after purification was sealed in glass tubes (250 μl) under an Ar atmosphere, and dipped into a water bath (stability of temperature, ±0.5 °C) which was covered with aluminium foil. Each tube was picked out at different delay times and the solution inside was directly subjected to HPLC analysis.

MM2 calculations

Optimized geometry of the all-*trans*, 7-*cis*, 9-*cis*, 11-*cis*, 13-*cis*, 15-*cis* and 11,11′-di-*cis* isomers of β-carotene in the gas phase at 0 K was predicted based on a classical molecular-mechanics calculation using the MM2 program incorporated into CS Chem3D pro ver. 3.5 (CambridgeSoft Corporation). The MM2 program used here adopted a modified version of Allinger's MM2 force-field;[34] parameters for bond-stretches, angle-bends, out-of-plane bends and torsions were transferred from the reported values of Brukert and Allinger.[34] Principal additions to the force-field are: (1) a charge–dipole interaction term, (2) cubic and quartic stretching terms, (3) a sextic bending term, (4) cutoffs for electrostatic and van der Waals terms with a fifth-order polynomial switching function, (5) π system calculations (a Pariser–Parr–Pople π orbital SCF computation in order to scale bond-stretching force constants, standard bond lengths, and twofold torsional barriers), and (6) torsional and non-bonded constraints. The relevant parameters were set as follows: the bond–dipole parameter of C–H bond to calculate the charge–dipole interaction energy, 0.300 Å V^{-1}; the cubic and quartic stretching constants, −2.000 $Å^{-1}$ and 2.333 $Å^{-2}$; the sextic bending constant, 7.000 × 10^{-8} rad^{-4}; the cutoff distances for charge–charge, charge–dipole, dipole–dipole, and van der Waals interactions, 35.000, 25.000, 18.000 and 10.000 Å, respectively; and stretch–bend force constants for C–C–C and C–C–H atom combinations, 0.120 and 0.090 mdyn $Å^{-1}$ rad^{-1}, respectively. The geometry optimization was initiated from a planar conformation for the conjugated backbone with the s-*cis* structures around the C6–C7 and C6′–C7′ bonds (we confirmed that an s-*trans* structure shows greater steric energy than that of the s-*cis* structure). The C_2 structure of the 11,11′-di-*cis* isomer was optimized starting from a C_2 structure based on the coordinates obtained for the C_i structure. The final convergence was achieved by setting the parameter of the minimum RMS gradient to be 0.01.

Acknowledgements

The authors would like to express deep appreciation for Dr Hiroyoshi Nagae's (Kobe University of Foreign Studies) support in performing the PPP-CI calculations of the model polyene. The authors thank Drs Yumiko Mukai and Hiroto Kikuchi for stimulating discussions and support in the normal-coordinate and PM3 calculations, and Dr Hiroyoshi Nagae and Dr Grazyna Ewa Bialek-Bylka for critical reading of the manuscript. This work has been supported by grant-in-aids (No. 06239101 to Y. K. and No. 08740251 to H. H.) from the Ministry of Education, Science and Culture in Japan, and also by a grant from the Human Frontier Science Program.

References

1 Y. Koyama, *J. Photochem. Photobiol. B: Biol.*, 1991, **9**, 265.
2 Y. Koyama and Y. Mukai, *Biomolecular Spectroscopy Part B*, *Advances in Spectroscopy*, ed. R. J. H. Clark and R. E. Hester, Wiley, New York, 1993, vol. 8, p. 49.
3 N. Ohashi, N. Ko-chi, M. Kuki, T. Shimamura, R. J. Cogdell and Y. Koyama, *Biospectrosc.*, 1996, **2**, 59.
4 G. E. Bialek-Bylka, T. Tomo, K. Satoh and Y. Koyama, *FEBS Lett.*, 1995, **363**, 137.
5 G. E. Bialek-Bylka, T. Hiyama, K. Yumoto and Y. Koyama, *Photosynth. Res.*, 1996, **49**, 245.
6 T. Yoshizawa and G. Wald, *Nature*, 1963, **197**, 1279.
7 R. S. Becker, *Photochem. Photobiol.*, 1988, **48**, 369.
8 L. Zechmeister, *Cis-Trans Isomeric Carotenoids*, *Vitamins A*, *and Arylpolyenes*, Academic Press, New York, 1962.
9 M. Denny and R. S. H. Liu, *J. Am. Chem. Soc.*, 1977, **99**, 4865.
10 (*a*) K. Tsukida, A. Kodama and M. Ito, *J. Chromatogr.*, 1977, **134**, 331; (*b*) V. Ramamurthy, M. Denny and R. S. H. Liu, *Tetrahedron Lett.*, 1981, **22**, 2463.
11 K. Tsukida and K. Saiki, *J. Nutr. Sci. Vitaminol.*, 1982, **28**, 311.
12 H. Hashimoto, Y. Miki, M. Kuki, T. Shimamura, H. Utsumi and Y. Koyama, *J. Am. Chem. Soc.*, 1993, **115**, 9216.
13 Y. Hu, A. Okumura, Y. Koyama, Y. Yamano and M. Ito, *Spectrochim. Acta Part A*, 1997, **53**, 913.
14 Y. Mukai, Y. Koyama, M. Ito and K. Tsukida, *J. Raman Spectrosc.*, 1986, **17**, 387.
15 Y. Hu, T. Mizoguchi, Y. Kurimoto and Y. Koyama, *Spectrochim. Acta Part A*, 1995, **51**, 1949.
16 K. Tsukida, K. Saiki, T. Takii and T. Koyama, *J. Chromatogr.*, 1982, **245**, 359.
17 Y. Koyama, T. Takii, K. Saiki and K. Tsukida, *Photobiochem. Photobiophys.*, 1983, **5**, 139.
18 Y. Koyama, I. Takatsuka, M. Nakata and M. Tasumi, *J. Raman Spectrosc.*, 1988, **19**, 37.
19 Y. Koyama, M. Hosomi, H. Hashimoto and T. Shimamura, *J. Mol. Struct.*, 1989, **193**, 185.
20 M. Kuki, Y. Koyama and H. Nagae, *J. Phys. Chem.*, 1991, **95**, 7171.
21 W. von E. Doering, C. Sotiriou-Leventis and W. R. Roth, *J. Am. Chem. Soc.*, 1995, **117**, 2747.
22 Y. Koyama, M. Hosomi, A. Miyata, H. Hashimoto, S. A. Reames, K. Nagayama, T. Kato-Jippo and T. Shimamura, *J. Chromatogr.*, 1988, **439**, 417.
23 S. Saito and M. Tasumi, *J. Raman Spectrosc.*, 1983, **14**, 310.
24 K. Iwata, H. Hayashi and M. Tasumi, *Biochim. Biophys. Acta*, 1985, **810**, 269.
25 (*a*) H. Günther, *NMR Spectroscopy 2nd edn.*, Wiley, Chichester, 1992; (*b*) E. Breitmaier and W. Voelter, *Carbon-13 NMR Spectroscopy 3rd edn.*, VCH Verlag, Weinheim, 1987.
26 (*a*) M. C. Bruni, J. P. Daudey, J. Langlet, J. P. Malrieu and F. Momicchioli, *J. Am. Chem. Soc.*, 1977, **99**, 3587; (*b*) V. Bonačić-Koutecký and S. Ishimaru, *J. Am. Chem. Soc.*, 1977, **99**, 8134; (*c*) M. Aoyagi, Y. Osamura and S. Iwata, *J. Chem. Phys.*, 1985, **83**, 1140.
27 K. J. Laidler and H. Eyring, *The Theory of Rate Processes*, McGraw-Hill, New York, 1964.
28 I. Agalidis, M. Lutz and F. Reiss-Husson, *Biochim. Biophys. Acta*, 1980, **589**, 264.
29 (*a*) H. Hopf and N. Krause, *Tetrahedron Lett.*, 1985, **26**, 3323; (*b*) P. A. Bütikofer and C. H. Eugster, *Helv. Chim. Acta*, 1983, **66**, 1148; (*c*) J.-L. Olivé, M. Mousseron-Canet and J. Dornand, *Bull. Soc. Chim. Fr.*, 1969, 3247.
30 V. L. Khristoforov, E. N. Zvonkova, V. P. Varlamov, O. N. Sorokina and R. P. Evstigneeva, *J. Org. Chem. USSR* (*Engl. Transl.*), 1973, **9**, 1868; *Zh. Org. Khim.*, 1973, **9**, 1844.
31 (*a*) A. Furuhata, H. Yokokawa and M. Matsui, *Agric. Biol. Chem.*, 1984, **48**, 3129; (*b*) A. Nürrenbach, J. Paust, H. Pommer, J. Schneider and B. Schulz, *Liebigs Ann. Chem.*, 1977, 1146.
32 O. Isler, L. H. Chopard-dit-Jean, M. Montavon, R. Rüegg and P. Zeller, *Helv. Chim. Acta*, 1957, **40**, 1256.
33 J. D. Surmatis, US Patent 3 367 985, 1966; *Chem. Abstr.*, 1968, **68**, 114 786.
34 U. Burkert and N. L. Allinger, *Molecular Mechanics*, ACS Monograph 177, American Chemical Society, Washington DC, 1982.

Paper 7/03763E
Received 30*th May* 1997
Accepted 11*th August* 1997